Noncovalent Functionalization and Passivation of Black Phosphorus with Optimized Perylene Diimides for Hybrid Field Effect Transistors

Vicent Lloret, Edurne Nuin, Malte Kohring, Stefan Wild, Mario Löffler, Christian Neiss, Michael Krieger, Frank Hauke, Andreas Görling, Heiko B. Weber, Gonzalo Abellán,* and Andreas Hirsch*

Amongst the different existing methods to passivate black phosphorus (BP) from environmental degradation, the noncovalent functionalization with perylene diimides (PDI) has been postulated as one of the most promising routes because it allows preserving its electronic properties. This work describes the noncovalent functionalization and outstanding environmental protection of BP with tailor made PDI having peri-amide aromatic side chains, which include phenyl and naphthyl groups, exhibiting a significantly increased molecule-BP interaction. These results are rationalized by density functional theory (DFT) calculations showing that the adsorption energies are mainly governed by van der Waals (vdW) interactions and increase concomitantly with the aromatic character of the side chains. The resulting hybrids are thoroughly characterized showing enhanced ambient and thermal stabilities. Last but not least, hybrid organic–inorganic BP-PDI field effect transistors (FETs) are studied for the first time showing the usefulness of PDI derivatives as efficient passivation layers while obtaining improved values of electron mobilities. These results pave the way for the use of optimized PDIs by molecular engineering to preserve the electronic properties of BP FETs, using straightforward wet chemical approaches.

1. Introduction

The post-graphene monoelemental 2D material black phosphorus (BP) has gained notable attention during the past years due to its outstanding physical and chemical properties.[1–2] Experimental studies have shown that BP-based field effect transistors (FETs) exhibit ambipolar electron/hole behavior while possessing advanced values in terms of the on/off ratio (10^6) and high carrier mobility (up to ≈ 1000 cm^2 V^{-1} s^{-1}). Moreover, the tuneable direct bandgap of the material (spanning from 0.3 eV in bulk to 2 eV for a monolayer) make it an excellent candidate for (opto)electronics.[1–8] Besides, its puckered structure with the free pair of electrons and its large chemically active surface area positions it as an excellent material in applications beyond electronics like gas sensing[9–13] and organic catalysis, among others.[14–15] Nevertheless, the biggest handicap of BP is its high oxophilicity, which turns its surface hydrophilic, promoting its decomposition to phosphoric acid species in presence of O_2 and H_2O.[16–19] Furthermore, it has been proven that the degradation of the material can be enhanced by photo-oxidation, due to the formation of highly reactive oxygen radicals.[20–22] Therefore, a large part of the research effort on BP is focused on alleviating its degradation in environmental conditions, avoiding oxidation and, consequently, facilitating its

V. Lloret, Dr. E. Nuin, S. Wild, Dr. F. Hauke, Dr. G. Abellán, Prof. A. Hirsch
Department of Chemistry and Pharmacy
Joint Institute of Advanced Materials and Processes (ZMP)
Friedrich-Alexander-Universität Erlangen-Nürnberg (FAU)
Nikolaus Fiebiger-Strasse 10, Erlangen 91058, Germany
E-mail: gonzalo.abellan@fau.de; andreas.hirsch@fau.de
Dr. E. Nuin, Dr. G. Abellán
Instituto de Ciencia Molecular (ICMol)
Universidad de Valencia
Catedrático José Beltrán 2, Paterna 46980, Spain

The ORCID identification number(s) for the author(s) of this article can be found under https://doi.org/10.1002/admi.202001290.

M. Kohring, Dr. M. Krieger, Prof. H. B. Weber
Department of Physics
Friedrich-Alexander-Universität Erlangen-Nürnberg (FAU)
Staudtstr. 7, Erlangen 91058, Germany
M. Löffler
Helmholtz Institute Erlangen-Nürnberg for Renewable Energy (IEK-11)
Forschungszentrum Jülich GmbH
Department of Chemical and Biological Engineering
Friedrich-Alexander-Universität Erlangen-Nürnberg (FAU)
Egerland-straße 3, Erlangen 91058, Germany
Dr. C. Neiss, Prof. A. Görling
Lehrstuhl für Theoretische Chemie
Friedrich-Alexander-Universität Erlangen-Nürnberg (FAU)
Egerlandstrasse 3, Erlangen 91058, Germany

application. Several pathways which include hybrid heterostructure encapsulation,[23–28] covalent modification,[29–36] solvent passivation,[9,37–38] or noncovalent functionalization[39–46] have been already studied leading to protected BP surfaces with disparate degrees of success. The first method has been mainly achieved by the coverage of single flakes/devices with thick inorganic layers which encapsulate BP up to 8 months but may promote impurities and defects negatively affecting its carrier mobility.[23] Regarding to the covalent functionalization, several groups have already reported the formation of P−C bonds but the BP layers tend to decompose within a few days due to the bridge oxygen incorporation within the layers, facilitated by the lattice P−P bond breaking taking place after the functionalization.[32,34] Moreover, the covalent functionalization of BP results in a change of the hybridization of P orbitals altering its intrinsic electronic properties.[47] Fortunately, the noncovalent functionalization mediated by weak interactions of molecules with BP offers a promising alternative route to protect BP preserving at the same time its electronic properties.

Among different molecules like high boiling point pyrrolidones,[9] ionic liquids (IL),[38,48] or strong electron acceptor molecules such as 7,7,8,8-tetracyano-p-quinodimethane (TCNQ), our groups reported the successful synthesis of BP-hybrids consisting of electron-poor and polarizable aromatic perylene diimide (PDI).[42,49] These hybrids are mainly formed spontaneously in solution due to strong van der Waals (vdW) interactions, and hold great promise for protecting BP from environmental degradation, as long as a minimum coating of 2 nm is reached with high order in the packaging of the molecules.[42,50] Previous theoretical and experimental studies suggested promising properties for optoelectronic devices such as improved photo-oxidation[49] and thermal stability,[42] or the preservation of its electronic bandgap–which offers the possibility of studying its intrinsic electronic properties without affecting the carrier mobility.[46] Moreover, developing an appropriate functionalization strategy could pave the way for a controlled doping of BP with organic molecules.[51–53]

In this sense, tailor made PDIs are suitable for the noncovalent functionalization of 2D materials due to their exceptional properties, which can be tuned by changing the substituents in the peri-position, affecting at the same time their vdW interaction and solubility in different solvents.[54] However, the development of environmentally stable low-dimensional organic/BP hybrid devices and the investigation of their electronic properties remains an open challenge.

Herein, we describe the synthesis of theoretically optimized tailor made perylene diimides, maximizing the molecule-BP interaction and allowing an outstanding environmental protection. These PDIs endowed with different peri-amide functionalized moieties, which include phenyl and naphthyl groups, exhibit an improved intermolecular interaction in the noncovalent functionalization of BP. The resulting hybrids have been fully characterized by absorbance, photoluminescence and scanning Raman microscopy correlated with atomic force microscopy (AFM). Moreover, environmental stability has been monitored by X-ray photoelectron spectroscopy (XPS) measurements confirming the formation of the BP-PDI hybrids and quantifying the evolution of BP oxidation with the time. Additionally, we demonstrated by means of temperature-dependent Raman and thermogravimetry coupled to mass spectrometry (TG-MS)

the usefulness of PDIs for achieving the thermal stabilization of 2D-BP both in its micromechanical and liquid phase exfoliated forms. Last but not least, hybrid organic-inorganic BP-PDI field effect transistors have been studied for the first time showing the usefulness of PDI derivatives as efficient passivation layers while obtaining improved values of electron mobilities.

These results demonstrate that noncovalent functionalization using straightforward wet chemistry is an effective approach for BP passivation, preserving the unique electronic properties of pristine BP in FET devices.

2. Results and Discussion

A recent work has shown that the PDI core, perylene tetracarboxylic dianhydride (PTCDA) can be sublimed and deposited onto a bulk BP surface controlling the number of passivating layers. The results prove that there is a charge transfer from BP valence band to PTCDA and that a thin film of the organic molecule can effectively isolate BP from reactive oxygen species, holding great promise in optoelectronic devices.[46] When it comes to conventional wet-chemical routes, the successful assembly of the PDI molecules on the BP surface is mostly limited by the periphery groups (mainly introduced for improving the low solubility of PDI derivatives), which may induce a poor packing of the molecules, thus restricting the effectiveness of passivation. Our hypothesis relies on the assumption that increasing the aromatic character of the periphery branches will improve the interaction with the BP surface, leading to a better molecular packing.

Herein, we have designed two PDI derivatives having an increasing number of π electrons as aromatic end-groups (namely benzene and naphthalene), in order to force the PDI peripheral moieties to strongly interact with the surface of BP. This is useful for improving the surface coating, allowing for a denser and more structured packing of the molecules (**Scheme 1**).[55] In addition, we compared these molecules with the N-bis-(tert-butyl-(2,2′-aminobutylazanediyl)-diacetate)-3,4,9,10-perylene diimide derivative previously reported by our group, which serves as an appropriate control experiment.[42,49]

Hence, according to **Scheme 2**, the synthetic approach started from the perylene-3,4,9,10-tetracarboxylic dianhydride (a). An imidization reaction of (a) with 1,4-diaminobutane in toluene at 118 °C provides the symmetrically N,N-substituted PDI (b) as a red solid with 45% yield.

Once (b) was afforded, the second part of the synthetic procedure consisted in the preparation of ethyl 4-(bromomethyl)-1-naphthoate. Thus, reaction of 4-methyl-1-naftholic acid (c) with EtOH at 78 °C in the presence of thionyl chloride provide (d) in quantitative yield, which was subsequently N-bromosuccinimide brominated in the presence of 2,2'-azobisisobutyronitrile giving rise to brominated derivative in 76% yield. Further reaction of (b) with ethyl 4-(bromomethyl)benzoate or ethyl 4-(bromomethyl)-1-naphthoate, was carried out to provide the PDI-R2 and PDI-R3 in good yields as red solids, respectively.

The role of the PDI peripheral substituents on the noncovalent functionalization of BP was first studied by density functional theory (DFT) calculations (see the Supporting Information for computational details). To this end, we have started by screening the influence of different terminal groups (i.e.,
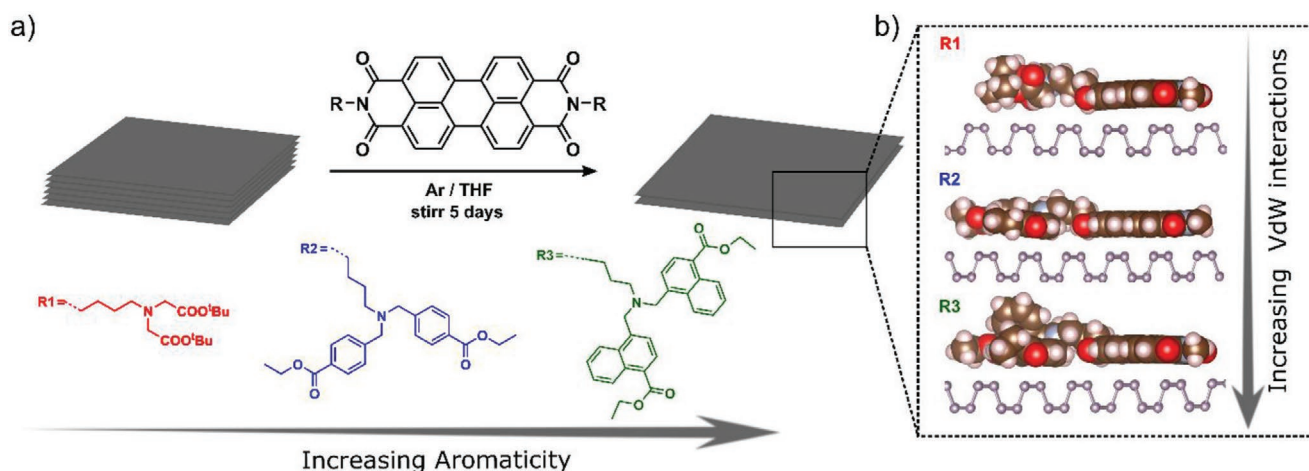
Scheme 1. a) General functionalization of micromechanically exfoliated/grounded BP by the use of perylene diimides with three different peripheral moieties containing aromatic groups (R1, R2, and R3). b) DFT optimized structures highlighting the interaction between the different PDIs and the BP surface.

alkyl, aromatic, and ester groups) on the adsorption energies and the charge transfer between PDIs and monolayer BP (Figure S1, Supporting Information). In all the cases, the total adsorption energies of each of the PDIs is a combination of the adsorption energy of the π-core and the side chain, but due to geometrical constraints in the linking region between the PDI core and the side chain, it is not the sum of the individual adsorption energies (Figures S2 and S3, Supporting Information).

While the presence of ester groups does not seem to affect much the interaction energy in the hybrid formation, the incorporation of aromatic groups shows a significantly larger binding energy between PDIs and BP (**Table 1**) as the interaction between BP and the PDI molecule is governed by vdW forces. Moreover, our results indicate that there is a slightly enhanced charge transfer from BP to PDIs containing ester groups, compared to those having alkyl chains. Nevertheless,
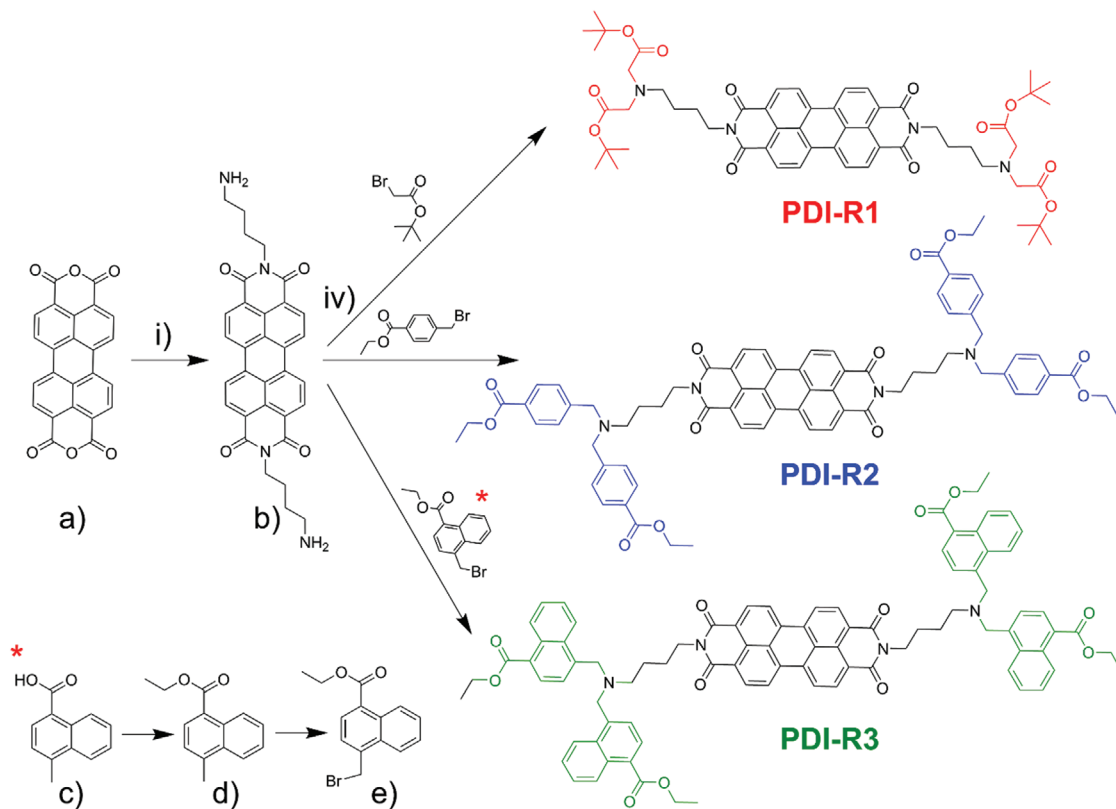
Scheme 2. Synthesis of PDI-2 and 3. Reagents and conditions i) Toluene, 1,4-diaminobutane, 118 °C, 4 h. ii) EtOH, thionyl chloride, 4-methyl-1-naphtholic acid, 80 °C, 12 h. iii) CHCl₃, N-bromosuccinimide, 2,2'-azobisisobutyronitrile, 62 °C, 4 h. iv) ACN, DIPEA, Br-derivative, 60 °C, 24 h.

Table 1. Adsorption energies, vdW contributions and Bader partial charges of BP-PDI hybrids.

	E_{ads} [eV]	vdW cont. [eV]	Charge ads.
R1	−2.78	−3.40	−0.15
R2	−3.40	−4.07	−0.13
R3	−3.70	−4.43	−0.14

the charge transfer is rather small and no simple correlation between the charge transfer and the adsorption energy is obtained (Figures S1–S3, Supporting Information).

Scheme 1b depicts the noncovalent functionalization of BP and the side-view images of the calculated hybrids highlighting the interaction of the PDI moieties with BP. It is possible to observe that the PDIs containing aromatic groups lie flat on the BP surface having a pronounced vdW interaction. The adsorption energies, vdW contributions to the adsorption energies and Bader partial charges of the adsorbed PDIs (R1–R3) are compiled in Table 1 (see Figure S1 (Supporting Information) for a complete list of all calculated PDI derivatives). The comparison of the listed values indicates that the naphthalene-containing PDI-R3 interacts most with BP, thus confirming our initial hypothesis.

Once we have theoretically validated the suitability of our molecules, we turn to study their behavior in solution. It is well known that the tuning of the peripheral substituents in the PDIs allows the modulation of inter and intramolecular forces leading to monomeric or aggregated (dimeric, trimeric) species. The strong π–π stacking of the planar core leads to slightly different H-aggregates showing disparate solubilities, which can be easily studied by UV/Vis and fluorescence spectroscopy.[54] Commonly, solvents such as chloroform, ortho-dichlorobenzene or dimethylsulphoxide (DMSO) are used for solubilizing perylenes (Figure S4, Supporting Information).[55] Moreover, our group previously reported the formation of labile charge transfer complexes (CTC) between perylene diimides and electron donating solvents like pyrrolidones or DMSO.[42] In this sense, THF is very convenient for the noncovalent functionalization of BP because it avoids the formation of CTCs under inert conditions, while allowing the spectroscopic characterization without extrinsic interferences.

Figure S5 (Supporting Information) shows the characteristic absorption spectrum of the studied PDIs (Scheme 1a) presenting the (0-0), (0-1), and (0-2) vibrational modes of the S_0-S_1 transition at 456, 485, and 521 nm, respectively. Both, PDI R1 and R2 exhibit an additional absorption band at 552 nm, which nearly vanishes for PDI R3 (Figure S5, Supporting Information). This band is related to the formation of different H-aggregates due to the strong vdW interactions of the core, therefore suggesting a monomeric behavior for the naphthyl derivative (PDI R3). In any case, fluorescence spectroscopy proves that the aggregation of all these systems is rather weak, showing three peaks with nearly identical intensity ratios for all PDIs, meaning that there are small aggregation differences in solution (Figure S5, Supporting Information).

The noncovalent functionalization of BP has been carried out using both micromechanically exfoliated flakes and bulk BP exfoliated in liquid phase. These wet chemical strategies allow
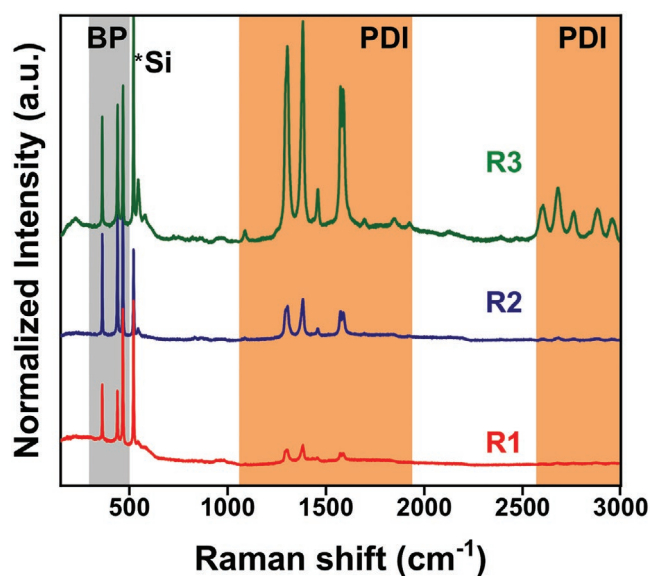

Figure 1. Normalized mean Raman spectra of the BP-PDI hybrids showing enhanced intensities for each of the perylene bands. The measured flakes exhibit the same heights in order to assure the correct comparison of the intensities.

to overcome some of the limitations typically associated to the thermal evaporation methods, such as using small molecules (because of the poor thermal stability of some organic moieties), hence broadening the range of organic ligands that can be studied.

For micromechanical exfoliated flakes, BP nanosheets deposited on SiO_2/Si surfaces were immersed in the different PDI solutions (M = 10^{-5}) for 5 days (Figures S6–S8, Supporting Information). After immersing the wafers in acetone and subsequent sonication for 1 min in order to remove possible PDI aggregates, a homogeneous and selective functionalization of BP was achieved as demonstrated by Raman spectroscopy (**Figures 1** and **2**). The thickness of the organic coating layers was statistically estimated by AFM measurements before and after the supramolecular interaction took place.

Figure 2c shows the AFM images obtained after the coating process. The average increase in thickness obtained by measuring BP flakes functionalized with PDI-R2 gave values of 1.1 ± 0.2 nm (Figures S6 and S8, Supporting Information) which is in agreement with the previous results obtained by coating BP with PDI-R1.[42,49] In the case of PDI-R3, the organic layer showed the highest thickness, and therefore an increased number of layers, with values of 1.7 ± 0.3 nm (Figures S7 and S8, Supporting Information).[56]

Raman spectroscopy is a powerful technique for analyzing the interface interaction between PDIs and BP. The Raman spectra of the hybrids contain both the characteristic bands of BP and the PDI as a consequence of the strong quenching of the photoluminescence (PL) of the PDI.[42,56–58] Interestingly, the intensity of the PDI bands varies depending on the peri-substituents of the core, concomitantly increasing with the aromatic character of the ligand. Thus, PDI-R3 exhibits the highest Raman intensity (between 2500 and 3000 cm^{-1}) compared to R2 and R1, which can be explained by stronger adsorption energies (Figure 1).
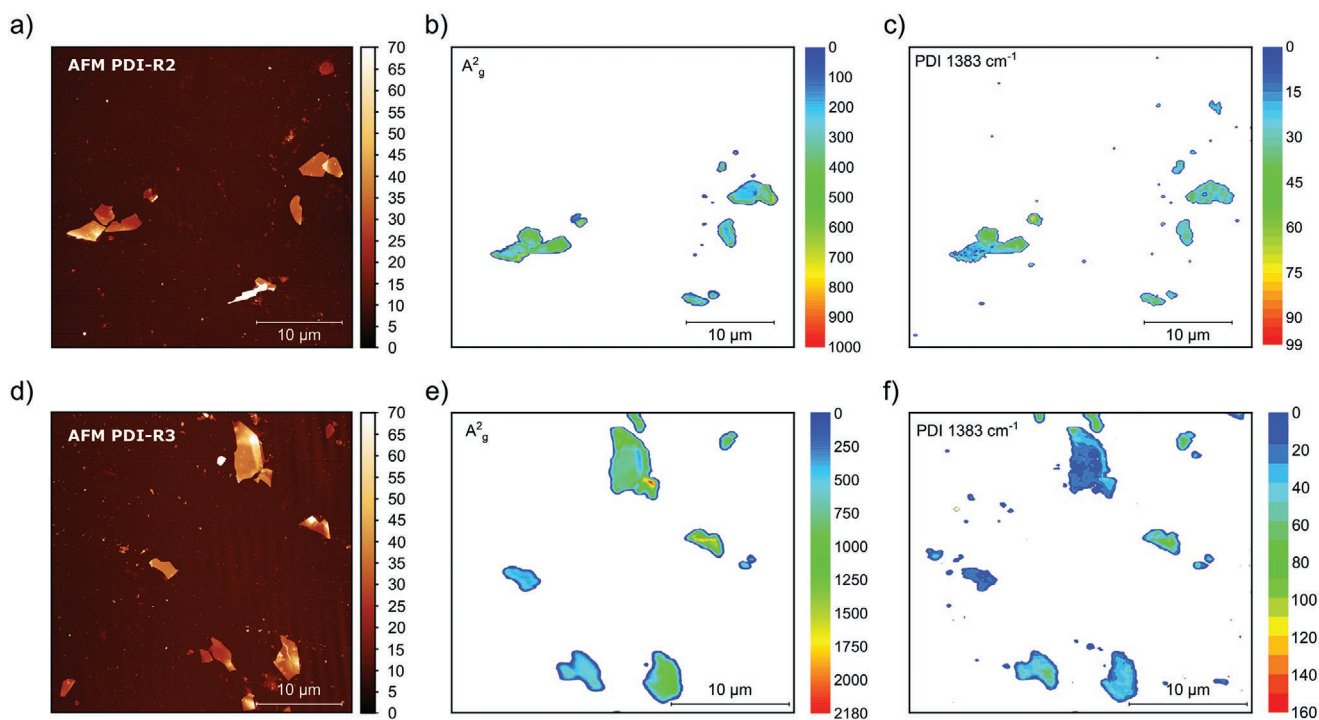
Figure 2. a) AFM images of the micromechanically exfoliated BP flakes after hybrid formation with PDI R2 (top) and R3 (bottom). SRM of the b) A^2_g BP and c) PDI representative Raman modes (1383 cm^{-1}) of BP-PDI R2 and e) A^2_g BP and f) PDI representative Raman modes (1383 cm^{-1}) modes of BP-PDI R3.

Raman maps of all the studied flakes were measured showing the BP modes at 361, 439, and 466 cm^{-1} and the characteristic PDI modes from 1086 to 3000 cm^{-1} (Figure 2d and Figures S6, S7, and S9, Supporting Information). Concerning the environmental stability of BP, as previously commented, a recent theoretical report determined that about 6 PTCDA (i.e., the core of the PDI molecule) monolayers ($\approx$1.3 nm) are the threshold for a complete passivation against oxygen and water penetration.[50] Taking into account our experimentally determined thicknesses of the organic layer, PDI R3 is well above this value, therefore suggesting an appropriate passivation behavior. The environmental stability of all samples was followed over time by AFM and scanning Raman microscopy (SRM). For this, BP flakes with similar thicknesses of $\approx$10 nm coated with the different PDIs were measured over time. The complete degradation of a pristine BP flake (10 nm thickness and 2 μm^2) is commonly reached after 72 h, with obvious signals of degradation (i.e., phosphoric acid bubble formation, etc.) after few hours.[38] In the case of PDI R1 hybrids, the BP flakes can be stabilized up to 7 days,[42,49] and when PDI R2 and R3 are used for the hybrid formation, the flakes survive at least for 22 days exposed to ambient moisture, presenting none, or only a slight degradation, successfully proving that the addition of aromatic moieties to the peri-position of the PDI increases the stability of BP. Even though the BP flakes remained intact for weeks (Figure 2d and Figure S6, Supporting Information), the intensity of the BP Raman modes can be further compared to analyze which one of the PDIs is able to protect better the surface of the material. Figure 2d proves that the intensity of the BP modes remains the same after 22 days in the case of

PDI-R3 but slightly decreases for R2, revealing that a higher stabilization is achieved for the BP-R3 hybrid (Figure S10, Supporting Information). In both cases, the A^1_g/A^2_g ratio remained over 0.4 suggesting that the material is not significantly oxidized (Figure S11, Supporting Information).[38] The oxidation of the BP-PDI R3 samples was also studied after 58 days. In this case, the thinner flakes (5 to 15 nm) show the formation of coalesced phosphoric acid bubbles but still, 30 nm thick flakes can be observed without traces of oxidation (Figure S12, Supporting Information), indicative of an effective passivation.

To better understand these hybrids and study their properties, we also explored the bulk exfoliation in liquids induced by the PDI molecules.[57–59] In this case the functionalization takes place on both sides of the flakes (antaratopic), in contrast to single-sided functionalization that takes place in micromechanically exfoliated flakes. Dispersions of the BP-PDI hybrids were prepared by mixing ground BP ($\approx$5 mg) in a 10^{-5} M solution of the respective PDI in THF. The dispersions were stirred for 5 days inside an Argon glove-box (<0.1 ppm H$_2$O and <0.1 ppm O$_2$) in quartz tubes in a carousel at controlled temperature (10 °C). This avoids solvent evaporation and thus, changes in the concentration of the perylenes (Figure 1a). After this time, the resultant dispersions exhibited Faraday–Tyndall effect, indicative of an efficient exfoliation (without ultra-sonication). Then, the samples were centrifuged for 30 min at 1000 rpm and aliquots of the dispersions were taken and sealed in a quartz cuvette to measure UV/Vis and fluorescence spectroscopy. As shown in Figure S13a,b (Supporting Information), an increase in the baseline of the UV/Vis measurements indicates a higher concentration of
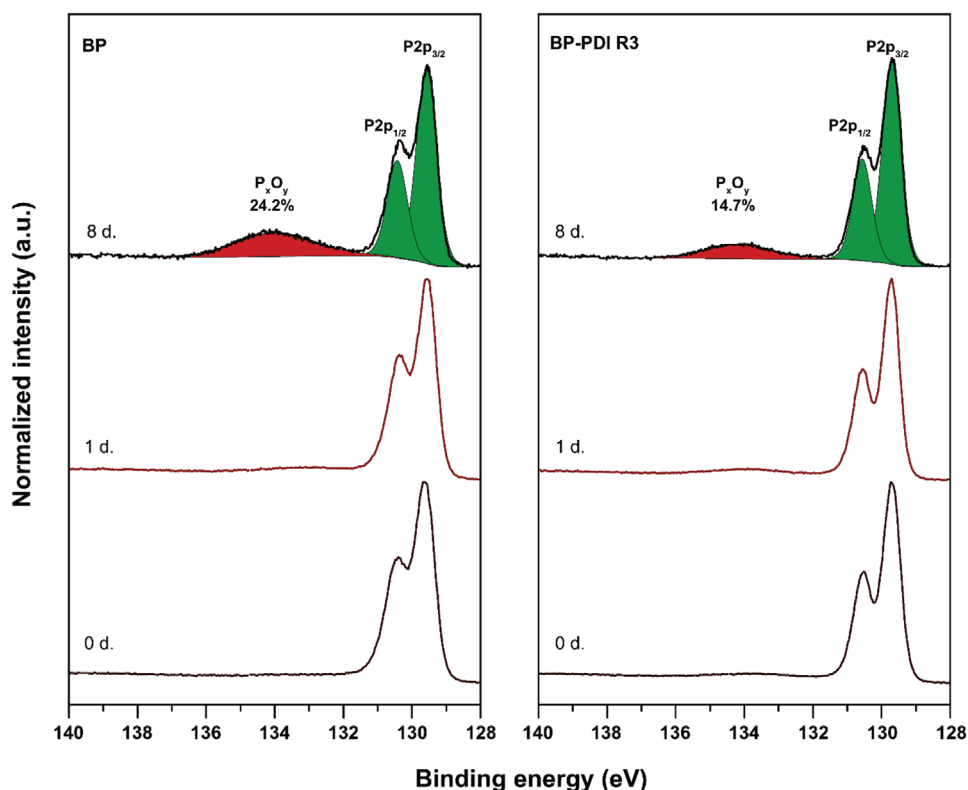
Figure 3. XPS measurements of BP (left) and BP-PDI R3 (right) over the time exposed to air. The areas of the BP and P-O peaks are stressed in green and red respectively showing an increase on the oxidation peaks in the pristine sample.

few layers (FL) BP in the dispersion. It is worth to remark here that when mono- and FL BP are present in the dispersions, characteristic absorption bands at 251 and 281 nm are observed, as corroborated with reference experiments of exfoliated BP in THF (Figure S14, Supporting Information). Moreover, as previously reported for BP or other 2D-materials such as graphene, fluorescence spectroscopy is a useful technique for studying how strong is the interaction between the perylenes and the 2D material. For PDI R1-BP hybrid, a similar quenching to the one obtained in graphene was achieved (≈66%).[42] Herein, the novel improved hybrids present quenching values of ≈90% and 98% for PDI R2 and R3, respectively (Figure S13, Supporting Information). To better understand the PL of the hybrids, emission–excitation contour maps of the BP-PDI dispersions in THF were obtained under Ar. The measurements give an overview of the PDI signals before and after interacting with BP, showing that the fluorescence of the perylenes is quenched (Figures S15 and S16, Supporting Information). Moreover, the typical PL of BP is not completely quenched, showing a small contribution that most likely stems from the existence of monolayer BP (Figure S16, Supporting Information).

The obtained dispersions were further characterized by AFM (Figures S17 and S18, Supporting Information). The dispersions were drop-casted on SiO_2/Si wafers, further sonicated (<1 min) and washed by spin coating several times with 2-propanol and acetone. Statistical AFM measurements show that in both cases the functionalized flakes exhibit relatively large micrometric sizes and thicknesses mainly comprised between 10 and 30 nm. Remarkably, even if the concentration of thin flakes in solution is small compared to conventional liquid phase exfoliation using tip sonication,[9] as shown by UV/Vis (Figure S13, Supporting Information), there are flakes with large micrometric lateral dimensions, which are commonly obtained only by micromechanical exfoliation (Figures S6–S9, Supporting Information). This is explained by the mild conditions of the BP exfoliation with PDIs, allowing to delaminate the BP layers from the bulk material without reducing its lateral size. Thus, by mixing BP powder with PDI R2/3 in THF and stirring for 5 days, large (1 to 3 μm) and relatively thin flakes (10 to 30 nm) can be easily obtained (Figures S17 and S18, Supporting Information).

The bulk synthesis of PDI-BP hybrids described above allows to perform XPS studies, which are of utmost importance to precisely quantify the surface oxidation of BP over time. For this, the dispersions obtained after 5 days stirring were filtrated and transferred to XPS holders in the glove-box. The measurements prove the presence of both BP and PDI with binding energies 400, 130 and 129 eV for N 1s, P $2P_{1/2}$, and P $2P_{3/2}$ respectively (Figure S19, Supporting Information). **Figure 3** shows that the functionalized samples present around ≈2% of the oxidized material in contrast to BP pristine (0.22%), probably due to the oxygen traces present in the solvent. The same spot of each sample was measured again after 1 day exposed to ambient conditions, showing an increase in the binding energy corresponding to the P—O bond up to 3.39%, 5.6%, and 4.20% in the case of R1, R2, and R3 samples, respectively (**Table 2**).

Table 2. Oxidation degree of a BP pristine sample and the different hybrids obtained by XPS measurements.

Degree of Oxidation %	$t = 0$ day	$t = 1$ day	$t = 8$ days
BP pristine	0.0	6.8	24.2
BP-PDI R1	2.8	3.7	25.9
BP-PDI R2	2.5	5.1	24.8
BP-PDI R3	3.1	3.7	14.7

Interestingly, after exposing the samples for 8 days to ambient conditions, in all the cases the surface oxidation degree increased up to 30% while in the case of R3, the oxidation degree increased only up to 14% (i.e., 11,6% with respect to the initial one, Figure S20, Supporting Information). In order to study the homogeneity of the oxidation degree after 8 days, three different spots for each of the samples were measured and compared, proving that the PDI coverage is homogeneous (Figure S21, Supporting Information). In this way, it can be concluded by XPS that by using PDI with ethyl-naphtoate moieties (R3), the oxidation process is slowed down by half achieving an increase in the stability of the material for longer periods of time.

Perylenes are well-known for their high thermal stability and could be great candidates for protecting BP against strong temperature changes. Along this front, we investigated the thermal behavior of both single flakes prepared by micromechanical exfoliation and by liquid exfoliation. On the one hand, the thermal stability of the hybrids prepared by liquid exfoliation was studied by thermogravimetry coupled to mass spectrometry (TG-MS). TG measurements show a difference in the decomposition temperature between pristine BP and PDI-BP hybrids (**Figure 4**c). Pristine BP thermally decomposes at ≈444 °C presenting four main characteristic mass fragments (P, P_2, P_3, and P_4) all in one acute mass loss (Figure 4b).[34] In turn, the protected hybrids are stabilized up to ≈475 °C, showing broad signals peaking at ≈600 °C, as a consequence of the PDI protection (Figure 4d and Figure S22, Supporting Information).

On the other hand, for the hybrids prepared by micromechanical exfoliation, temperature dependent SRM was measured for pristine flakes and the corresponding noncovalently functionalized samples. This method allows to study small changes of temperature on single flakes functionalized on the top surface (supratopic), exactly determining the stability of the individual hybrids. While FL-BP pristine flakes (15 nm) are stable up to ≈200 °C, the noncovalently functionalized samples show an increase in the thermal stability up to ≈275 °C (PDI R3). The differences in the Raman spectra can be observed in **Figure 5** with a comparison of all samples. The disparities between the decomposition temperatures of single flake hybrids (SRM) and liquid exfoliated flakes (TG-MS) can be explained by a cooperative effect produced by the stacking/aggregation of
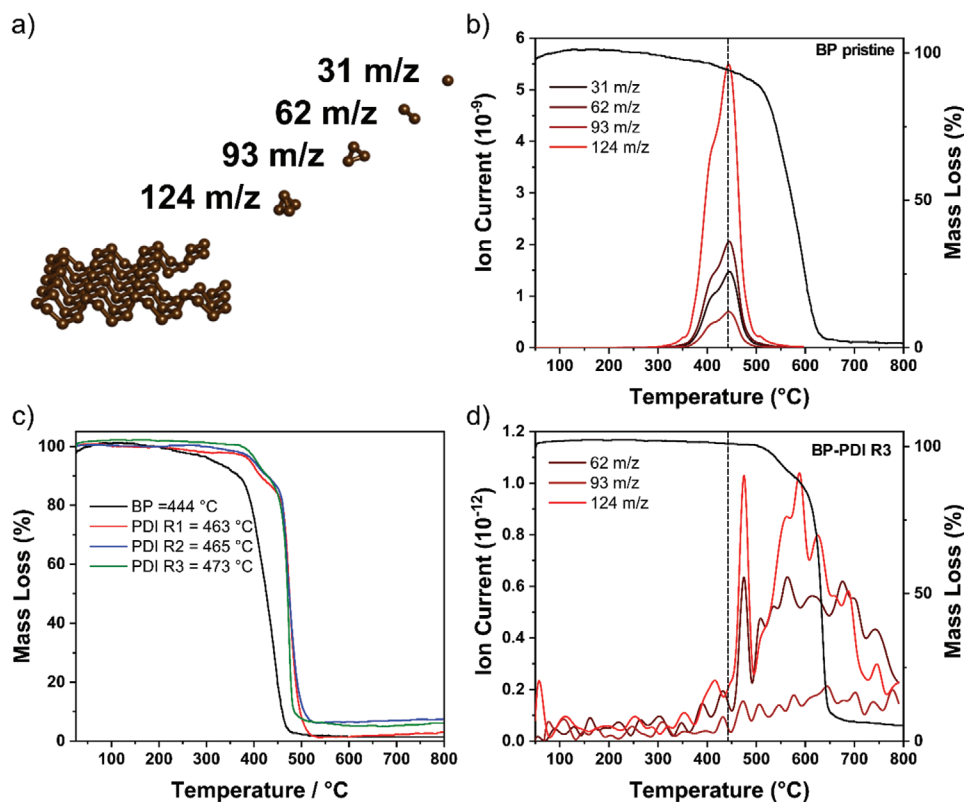

Figure 4. TG-MS measurements. a) Scheme representing the main BP fragments obtained by heating BP at 450 °C (P, P_2, P_3, and P_4). b) Ion current of the sub-products formed from the decomposition of BP. c) Mass loss of the samples BP pristine powder and the hybrids BP-PDI R1 to R3 showing an increase in the decomposition temperature of BP when protected with PDIs. d) Ion current of the sub-products formed from the decomposition of BP-PDI R3.
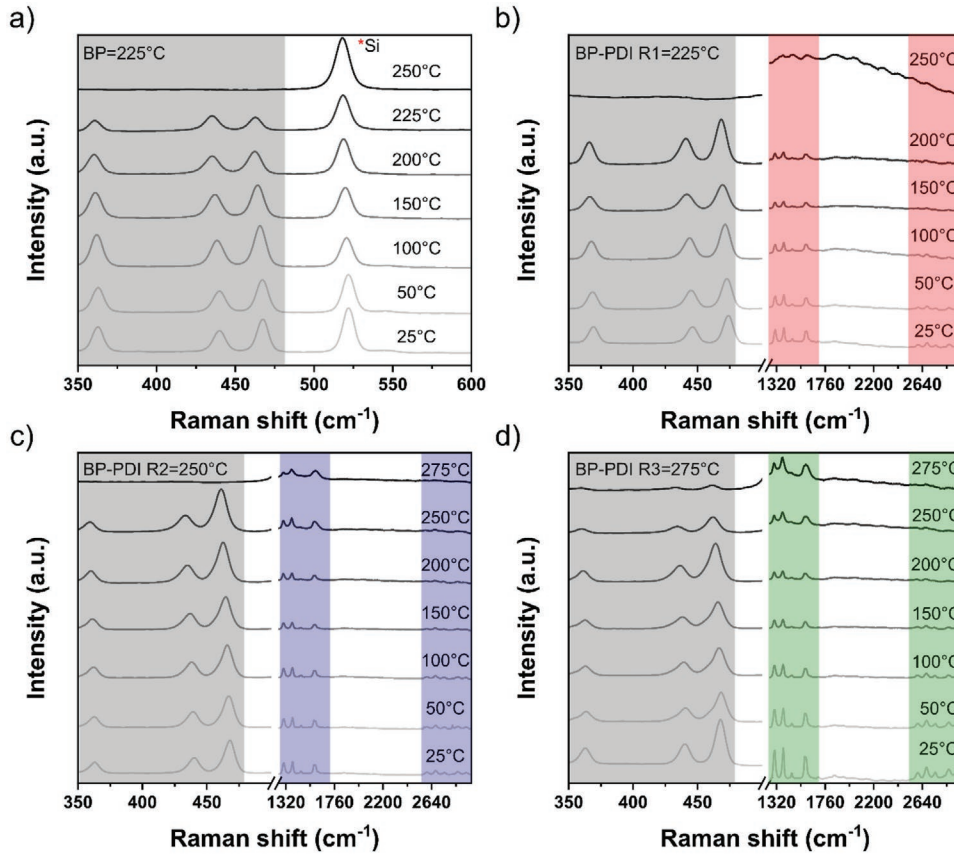
Figure 5. a) Raman temperature dependence of a micromechanically exfoliated BP flake with a decomposition temperature of 200 °C. b) T-dependent Raman spectra of BP-PDI R1 (225 °C), c) BP-PDI R2 (250 °C) and d) BP-PDI R3 (275 °C) hybrids.

the BP-PDI-BP-PDI hybrids after the filtration. Overall, these measurements nicely demonstrate that PDIs are not only able to stabilize BP against its ambient decomposition, but also against heating, which could be extremely relevant for nanodevice applications.

Last but not least, once we have demonstrated the suitability of PDIs as passivating agents, we can face the fabrication of environmentally stable hybrid BP FETs.[60–62] To this end, micromechanically exfoliated BP was obtained in the glove-box and transferred to a SiO_2/Si wafer which was previously equipped with a position marker system and a gold pad on the back side for contacting the silicon bulk. The formation of the BP-PDI-R3 hybrid was achieved following the previously described procedure, and was characterized by AFM and Raman spectroscopy and contacted using a FET configuration (**Figure 6**). Figure 6c displays 4-probe current–voltage (*I–V*) curves recorded for various gate voltages V_G. The curves are perfectly linear and show a clear gate response. Moreover, all individual contacts as evidenced from 2-probe measurements behave perfectly ohmic (linear *I–V*, not shown here). Therefore, the contact properties do not contribute significantly to the electrical measurements and are not discussed further. The flake's 4-probe resistance ranges from 12 kΩ (on-state) to 2.6 MΩ (off-state). The 4-probe conductance $\frac{dI_{SD}}{dV_{4p}}$ as a function of the gate voltage V_G is displayed in Figure 6d. Starting at $V_G = 0$ V, the flake is depleted when sweeping the

gate voltage toward +100 V (off-state). Thus, the sign of the gate voltage confirms that positive free charge carriers govern the electrical current in the BP flake. When the gate voltage is then swept to −100 V, the on-state is re-established, however, a hysteresis is formed and the current is larger than initially. The conductance increases linearly with decreasing gate voltage (for $V_G < 30$ V). Finally, we sweep back to 0 V. After a few data points, the conductance decreases again linearly with the same slope as for the down-sweep. Notably, the conductance at 0 V after the sweep cycle perfectly matches the initial value before the sweep. This suggests that this point is particularly meaningful and has little memory of the preceding process, except that the applied gate voltages have been sufficiently large to switch from the up-sweep (blue) to the down-sweep (red) curve. This switching between two curves suggests that the PDI molecules play a significant role in the charge balance by changing their charge state. The process is schematically displayed in Figure 6e, which represents the up-sweep/down-sweep cycle. Assuming that the PDI molecules are initially uncharged, positive charge carriers in the flake are depleted by the field effect when increasing the gate voltage starting from zero (blue branch), finally allowing to even negatively charge the PDI. As a result, the system evolves to the red branch. The charged PDI serves as an additional static gate and, consequently, additional positive charge carriers in the flake are available when sweeping the gate voltage toward negative voltages. This becomes measurable as a higher current in
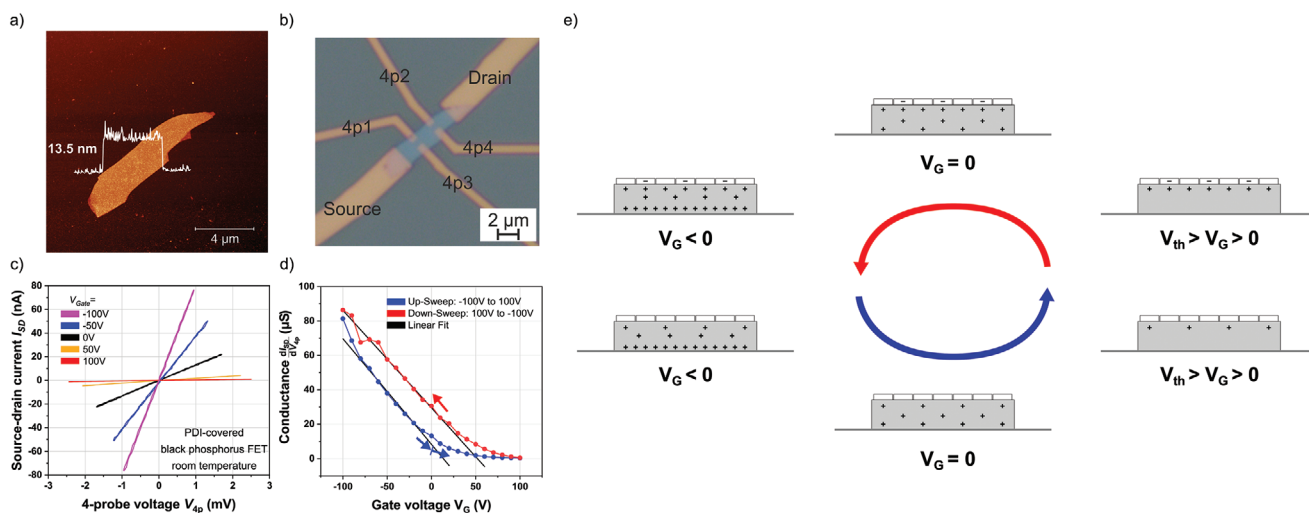
Figure 6. a) Topography AFM image of the of the electrically investigated BP flake before processing. The height profile is shown as overlay in the image. b) Microscope image of the processed BP field-effect transistor. The current is sent through the source and drain contacts while the 4-probe voltage is measured between the contacts 4p1 and 4p2. c) 4-probe current–voltage (*I–V*) measurements on a BP field-effect transistor for various gate voltages (each curve is averaged over 5 consecutive measurements). All *I–V* characteristics are perfectly linear. From the slopes the gate-dependent conductance is obtained and displayed in d). The gate-voltage sweep presents a hysteresis with two branches (blue and red curves) with a seamless closure at $V_G = 0$ V. e) Proposed model of the hysteretic charge balance cycle of PDI-covered BP flakes: only when significant depletion is achieved (V_G positive and large), the field effect also acts on the PDI molecules leading to negative charging and the creation of the down-sweep branch (red). The PDI molecules discharge when V_G is both negative and large. There, the system returns to the up-sweep branch (blue).

down-sweep direction. The opposite effect happens when the gate voltage is sufficiently negative ($V_G < -80$ V): the PDI is discharged and the static gate effect vanishes; the system switches back to the blue branch. Although this model can explain the observed hysteresis, it could also be attributed to interface traps between the silicon dioxide and the BP flake. However, the seamless connection of the hysteresis curve after a sweep cycle and the necessity of large gate voltages for switching to the other branch are untypical for interface traps. They rather point to charging of the flake side facing away from the gate electrode.

From the slope of the linear region, a charge carrier mobility of $\mu_{FE} = (130\ldots140)\frac{cm^2}{Vs}$ is calculated under the assumption of a field-effect induced charge carrier concentration. These values agree well when applying the different evaluation scheme for effective mobilities: here, the threshold voltage values $V_{th,\,up-sweep} = 14$ V or $V_{th,\,down-sweep} = 52$ V obtained from the intercept of the linear extrapolation with $\frac{dI_{SD}}{dV_{4p}} = 0$ µS are employed. The consistent values from the different evaluation schemes on both branches and the seamless closure of the hysteresis curve at zero volt give confidence that the system is intact and operates close to the textbook case of a field-effect transistor. The absolute values of mobilities, however, should be taken cum grano salis, with uncertainties due to the imperfect contact geometry (e.g., irregular flake geometry, flake thickness variations, nonpoint like electrical probes). Nevertheless, the results compare well with recent data obtained on differently processed BP flakes showing improved electron mobility.[29,49,63] These results corroborate that the use of PDI optimized by molecular engineering are optimal to preserve the electronic properties of BP.

3. Conclusion

The noncovalent functionalization and passivation of few-layer BP flakes with optimized PDIs having tailor made aromatic periphery chains has been achieved. Our theoretical and experimental results show that the inclusion of the aromatic moieties leads to higher adsorption energies mainly governed by van der Waals interactions, thus leading to a denser packing of the molecules on the BP surface. This is reflected in improved environmental and thermal stabilities, as demonstrated by XPS, temperature-dependent Raman spectroscopy and TG-MS. Finally, we studied for the first time the electronic properties of these hybrids by constructing PDI-BP field effect transistors showing a hysteretic charge balance behavior. The preservation of the electronic properties of BP is reflected in the values of charge carrier mobilities comprised in the 130–140 cm^2 V^{-1} s^{-1} range. This work highlights the noncovalent functionalization with PDIs as a very promising route for both environmental and electronic properties preservation, laying the grounds for the development of stable electronic devices based on functionalized 2D-pnictogens.

Supporting Information

Supporting Information is available from the Wiley Online Library or from the author.

Acknowledgements

Conflict of Interest

The authors declare no conflict of interest.

Keywords

black phosphorus, noncovalent functionalization, organic field effect transistors, perylene diimides

[1] X. Ling, H. Wang, S. Huang, F. Xia, M. S. Dresselhaus, *Proc. Natl. Acad. Sci. USA* **2015**, *112*, 4523.

[2] A. C. Ferrari, F. Bonaccorso, V. Fal'ko, K. S. Novoselov, S. Roche, P. Boggild, S. Borini, F. H. Koppens, V. Palermo, N. Pugno, J. A. Garrido, R. Sordan, A. Bianco, L. Ballerini, M. Prato, E. Lidorikis, J. Kivioja, C. Marinelli, T. Ryhanen, A. Morpurgo, J. N. Coleman, V. Nicolosi, L. Colombo, A. Fert, M. Garcia-Hernandez, A. Bachtold, G. F. Schneider, F. Guinea, C. Dekker, M. Barbone, Z. Sun, C. Galiotis, A. N. Grigorenko, G. Konstantatos, A. Kis, M. Katsnelson, L. Vandersypen, A. Loiseau, V. Morandi, D. Neumaier, E. Treossi, V. Pellegrini, M. Polini, A. Tredicucci, G. M. Williams, B. H. Hong, J. H. Ahn, J. M. Kim, H. Zirath, B. J. van Wees, H. van der Zant, L. Occhipinti, A. Di Matteo, I. A. Kinloch, T. Seyller, E. Quesnel, X. Feng, K. Teo, N. Rupesinghe, P. Hakonen, S. R. Neil, Q. Tannock, T. Löfwander, J. Kinaret, *Nanoscale* **2015**, *7*, 4598.

[3] J. D. Wood, S. A. Wells, D. Jariwala, K. S. Chen, E. Cho, V. K. Sangwan, X. Liu, L. J. Lauhon, T. J. Marks, M. C. Hersam, *Nano Lett.* **2014**, *14*, 6964.

[4] A. Castellanos-Gomez, L. Vicarelli, E. Prada, J. O. Island, K. L. Narasimha-Acharya, S. I. Blanter, D. J. Groenendijk, M. Buscema, G. A. Steele, J. V. Alvarez, H. W. Zandbergen, J. J. Palacios, H. S. J. van der Zant, *2D Mater.* **2014**, *1*, 025001.

[5] M. Buscema, D. J. Groenendijk, G. A. Steele, H. S. van der Zant, A. Castellanos-Gomez, *Nat. Commun.* **2014**, *5*, 4651.

[6] J. Qiao, X. Kong, Z. X. Hu, F. Yang, W. Ji, *Nat. Commun.* **2014**, *5*, 4475.

[7] F. Xia, H. Wang, Y. Jia, *Nat. Commun.* **2014**, *5*, 4458.

[8] L. Li, Y. Yu, G. J. Ye, Q. Ge, X. Ou, H. Wu, D. Feng, X. H. Chen, Y. Zhang, *Nat. Nanotechnol.* **2014**, *9*, 372.

[9] D. Hanlon, C. Backes, E. Doherty, C. S. Cucinotta, N. C. Berner, C. Boland, K. Lee, A. Harvey, P. Lynch, Z. Gholamvand, S. Zhang, K. Wang, G. Moynihan, A. Pokle, Q. M. Ramasse, N. McEvoy, W. J. Blau, J. Wang, G. Abellan, F. Hauke, A. Hirsch, S. Sanvito, D. D. O'Regan, G. S. Duesberg, V. Nicolosi, J. N. Coleman, *Nat. Commun.* **2015**, *6*, 8563.

[10] R. Jain, Y. Singh, S. Y. Cho, S. P. Sasikala, S. H. Koo, R. Narayan, H. T. Jung, Y. Jung, S. O. Kim, *Chem. Mater.* **2019**, *31*, 2786.

[11] L. Kou, T. Frauenheim, C. Chen, *J. Phys. Chem. Lett.* **2014**, *5*, 2675.

[12] Y. Q. Cai, Q. Q. Ke, G. Zhang, Y. W. Zhang, *J. Phys. Chem. C* **2015**, *119*, 3102.

[13] Y. Y. Zhang, C. Liu, F. Hao, H. Xiao, S. W. Zhang, X. Chen, *Appl. Surf. Sci.* **2017**, *397*, 206.

[14] V. Lloret, M. A. Rivero-Crespo, J. A. Vidal-Moya, S. Wild, A. Doménech-Carbó, B. S. J. Heller, S. Shin, H. P. Steinrück, F. Maier, F. Hauke, M. Varela, A. Hirsch, A. Leyva-Pérez, G. Abellán, *Nat. Commun.* **2019**, *10*, 509.

[15] M. Tejeda-Serrano, V. Lloret, B. G. Márkus, F. Simon, F. Hauke, A. Hirsch, A. Doménech-Carbó, G. Abellán, A. Leyva-Pérez, *ChemCatChem* **2020**, *12*, 2226.

[16] Y. Huang, J. Qiao, K. He, S. Bliznakov, E. Sutter, X. Chen, D. Luo, F. Meng, D. Su, J. Decker, W. Ji, R. S. Ruoff, P. Sutter, *Chem. Mater.* **2016**, *28*, 8330.

[17] J. O. Island, G. A. Steele, H. S. J. van der Zant, A. Castellanos-Gomez, *2D Mater.* **2015**, *2*, 011002

[18] J. Kang, J. D. Wood, S. A. Wells, J. H. Lee, X. Liu, K. S. Chen, M. C. Hersam, *ACS Nano* **2015**, *9*, 3596.

[19] S. Zhang, X. Zhang, L. Lei, X. F. Yu, J. Chen, C. Ma, F. Wu, Q. Zhao, B. Xing, *Angew. Chem., Int. Ed.* **2019**, *58*, 467.

[20] A. Favron, E. Gaufrès, F. Fossard, A. L. Phaneuf-L'Heureux, N. Y. Tang, P. L. Lévesque, A. Loiseau, R. Leonelli, S. Francoeur, R. Martel, *Nat. Mater.* **2015**, *14*, 826.

[21] K. L. Kuntz, R. A. Wells, J. Hu, T. Yang, B. Dong, H. Guo, A. H. Woomer, D. L. Druffel, A. Alabanza, D. Tomanek, S. C. Warren, *ACS Appl. Mater. Interfaces* **2017**, *9*, 9126.

[22] Q. Zhou, Q. Chen, Y. Tong, J. Wang, *Angew. Chem., Int. Ed.* **2016**, *55*, 11437.

[23] J. Pei, X. Gai, J. Yang, X. Wang, Z. Yu, D. Y. Choi, B. Luther-Davies, Y. Lu, *Nat. Commun.* **2016**, *7*, 10450.

[24] X. Chen, Y. Wu, Z. Wu, Y. Han, S. Xu, L. Wang, W. Ye, T. Han, Y. He, Y. Cai, N. Wang, *Nat. Commun.* **2015**, *6*, 7315.

[25] S. Gamage, A. Fali, N. Aghamiri, L. Yang, P. D. Ye, Y. Abate, *Nanotechnology* **2017**, *28*, 265201.

[26] J. S. Kim, Y. Liu, W. Zhu, S. Kim, D. Wu, L. Tao, A. Dodabalapur, K. Lai, D. Akinwande, *Sci. Rep.* **2015**, *5*, 8989.

[27] L. Hu, J. Yuan, Y. Ren, Y. Wang, J. Q. Yang, Y. Zhou, Y. J. Zeng, S. T. Han, S. C. Ruan, *Adv. Mater.* **2018**, *30*, 9383.

[28] B. Han, Z. H. Duan, J. Xu, Y. X. Zhu, Q. C. Xu, H. Wang, H. L. Tai, J. Weng, Y. L. Zhao, *Adv. Funct. Mater.* **2020**, *30*, 2002232.

[29] C. R. Ryder, J. D. Wood, S. A. Wells, Y. Yang, D. Jariwala, T. J. Marks, G. C. Schatz, M. C. Hersam, *Nat. Chem.* **2016**, *8*, 597.

[30] Z. Sofer, J. Luxa, D. Bousa, D. Sedmidubský, P. Lazar, T. Hartman, H. Hardtdegen, M. Pumera, *Angew. Chem., Int. Ed.* **2017**, *56*, 9891.

[31] Y. Cao, X. Tian, J. Gu, B. Liu, B. Zhang, S. Song, F. Fan, Y. Chen, *Angew. Chem., Int. Ed.* **2018**, *57*, 4543.

[32] M. van Druenen, F. Davitt, T. Collins, C. Glynn, C. O'Dwyer, J. D. Holmes, G. Collins, *Chem. Mater.* **2018**, *30*, 4667.

[33] H. Hu, H. Gao, L. Gao, F. Li, N. Xu, X. Long, Y. Hu, J. Jin, J. Ma, *Nanoscale* **2018**, *10*, 5834.

[34] S. Wild, M. Fickert, A. Mitrovic, V. Lloret, C. Neiss, J. A. Vidal-Moya, M. A. Rivero-Crespo, A. Leyva-Pérez, K. Werbach, H. Peterlik, M. Grabau, H. Wittkämper, C. Papp, H. P. Steinrück, T. Pichler, A. Görling, F. Hauke, G. Abellán, A. Hirsch, *Angew. Chem., Int. Ed.* **2019**, *58*, 5763.

[35] C. Su, Z. Y. Yin, Q. B. Yan, Z. G. Wang, H. T. Lin, L. Sun, W. S. Xu, T. Yamada, X. Ji, N. Zettsu, K. Teshima, J. H. Warner, M. Dinca, J. J. Hu, M. D. Dong, G. Su, J. Kong, J. Li, *Proc. Natl. Acad. Sci. USA* **2019**, *116*, 20844.

[36] S. C. Yan, H. Z. Song, L. F. Wan, S. R. Lin, H. Wu, Y. Sho, J. Yao, *Nano Lett.* **2020**, *20*, 81.

[37] Z. Sun, Y. Zhang, H. Yu, C. Yan, Y. Liu, S. Hong, H. Tao, A. W. Robertson, Z. Wang, A. A. H. Padua, *Nanoscale* **2018**, *10*, 12543.

[38] G. Abellán, S. Wild, V. Lloret, N. Scheuschner, R. Gillen, U. Mundloch, J. Maultzsch, M. Varela, F. Hauke, A. Hirsch, *J. Am. Chem. Soc.* **2017**, *139*, 10432.

[39] R. Guo, Y. Zheng, Z. R. Ma, X. Lian, H. C. Sun, C. Han, H. H. Ding, Q. Xu, X. J. Yu, J. F. Zhu, W. Chen, *Appl. Surf. Sci.* **2019**, *496*, 143688

[40] V. V. Korolkov, I. G. Timokhin, R. Haubrichs, E. F. Smith, L. Yang, S. Yang, N. R. Champness, M. Schröder, P. H. Beton, *Nat. Commun.* **2017**, *8*, 1385.

[41] H. Ghodrati, N. Antonatos, Z. Sofer, *Small* **2019**, *15*, 1903495.

[42] G. Abellán, V. Lloret, U. Mundloch, M. Marcia, C. Neiss, A. Görling, M. Varela, F. Hauke, A. Hirsch, *Angew. Chem., Int. Ed.* **2016**, *55*, 14557.

[43] M. Bolognesi, S. Moschetto, M. Trapani, F. Prescimone, C. Ferroni, G. Manca, A. Ienco, S. Borsacchi, M. Caporali, M. Muccini, M. Peruzzini, M. Serrano-Ruiz, L. Calucci, M. A. Castriciano, S. Toffanin, *ACS Appl. Mater. Interfaces* **2019**, *11*, 22637.

[44] C. Wang, D. M. Niu, Y. Zhao, S. T. Wang, C. Qian, H. Huang, H. P. Xie, Y. L. Gao, *J. Phys. Chem. C* **2019**, *123*, 10443.

[45] P. Vishnoi, S. Rajesh, S. Manjunatha, A. Bandyopadhyay, M. Barua, S. K. Pati, C. N. R. Rao, *ChemPhysChem* **2017**, *18*, 2985.

[46] C. Wang, D. M. Niu, B. X. Liu, S. T. Wang, X. H. Wei, Y. Q. Liu, H. P. Xie, Y. L. Gao, *J. Phys. Chem. C* **2017**, *121*, 18084.

[47] A. Hirsch, F. Hauke, *Angew. Chem., Int. Ed.* **2018**, *57*, 4338.

[48] S. Walia, S. Balendhran, T. Ahmed, M. Singh, C. El-Badawi, M. D. Brennan, P. Weerathunge, M. N. Karim, F. Rahman, A. Rassell, J. Duckworth, R. Ramanathan, G. E. Collis, C. J. Lobo, M. Toth, J. C. Kotsakidis, B. Weber, M. Fuhrer, J. M. Dominguez-Vera, M. J. S. Spencer, I. Aharonovich, S. Sriram, M. Bhaskaran, V. Bansal, *Adv. Mater.* **2017**, *29*, 1700152.

[49] S. Wild, V. Lloret, V. Vega-Mayoral, D. Vella, E. Nuin, M. Siebert, M. Koleśnik-Gray, M. Löffler, K. J. J. Mayrhofer, C. Gadermaier, V. Krstić, F. Hauke, G. Abellán, A. Hirsch, *RSC Adv.* **2019**, *9*, 3570.

[50] Y. Zhao, Q. Zhou, Q. Li, X. Yao, J. Wang, *Adv. Mater.* **2017**, *29*, 1603990.

[51] D. Xiang, C. Han, J. Wu, S. Zhong, Y. Y. Liu, J. D. Lin, X. A. Zhang, W. P. Hu, B. Ozyilmaz, A. H. C. Neto, A. T. S. Wee, W. Chen, *Nat. Commun.* **2015**, *6*, 6485.

[52] B. C. Yang, B. S. Wan, Q. H. Zhou, Y. Wang, W. T. Hu, W. M. Lv, Q. Chen, Z. M. Zeng, F. S. Wen, J. Y. Xiang, S. J. Yuan, J. L. Wang, B. S. Zhang, W. H. Wang, J. Y. Zhang, B. Xu, Z. S. Zhao, Y. J. Tian, Z. Y. Liu, *Adv. Mater.* **2016**, *28*, 9408.

[53] X. Z. Bao, Q. D. Ou, Z. Q. Xu, Y. P. Zhang, Q. L. Bao, H. Zhang, *Adv. Mater. Technol.* **2018**, *3*, 1800072.

[54] F. Würthner, C. R. Saha-Moller, B. Fimmel, S. Ogi, P. Leowanawat, D. Schmidt, *Chem. Rev.* **2016**, *116*, 962.

[55] E. Nuin, V. Lloret, K. Amsharov, F. Hauke, G. Abellán, A. Hirsch, *Chem. - Eur. J.* **2018**, *24*, 4671.

[56] M. Marcia, C. Vinh, C. Dolle, G. Abellán, J. Schönamsgruber, T. Schunk, B. Butz, E. Spiecker, F. Hauke, A. Hirsch, *Adv. Mater. Interfaces* **2016**, *3*, 1600365.

[57] G. Abellán, P. Ares, S. Wild, E. Nuin, C. Neiss, D. R. Miguel, P. Segovia, C. Gibaja, E. G. Michel, A. Görling, F. Hauke, J. Gómez-Herrero, A. Hirsch, F. Zamora, *Angew. Chem., Int. Ed.* **2017**, *56*, 14389.

[58] A. Hirsch, J. M. Englert, F. Hauke, *Acc. Chem. Res.* **2013**, *46*, 87.

[59] C. Gibaja, D. Rodriguez-San-Miguel, P. Ares, J. Gómez-Herrero, M. Varela, R. Gillen, J. Maultzsch, F. Hauke, A. Hirsch, G. Abellán, F. Zamora, *Angew. Chem., Int. Ed.* **2016**, *55*, 14345.

[60] F. Xia, D. B. Farmer, Y. M. Lin, P. Avouris, *Nano Lett.* **2010**, *10*, 715.

[61] I. Meric, M. Y. Han, A. F. Young, B. Ozyilmaz, P. Kim, K. L. Shepard, *Nat. Nanotechnol.* **2008**, *3*, 654.

[62] J. S. Miao, L. Zhang, C. Wang, *2D Mater.* **2019**, *6*, 032003.

[63] S. Kim, J. Y. Lee, C. H. Lee, G. H. Lee, J. Kim, *ACS Appl. Mater. Interfaces* **2017**, *9*, 21382.